Natural Resources for Human Health
eISSN: 2583-1194

Original Research

Received 20 July 2026
Revised 28 Aug 2026
Accepted 10 Sep 2026

Natural Resources for Human Health 2026, Vol. 6 (22s): 1211–1230

KEYWORDS:
Diabetic wound healing; Moringa concanensis; Interleukin-7; Kaempferol; Network pharmacology; Molecular dynamics simulation

Therapeutic Potential of Moringa concanensis in Diabetic Wound Healing: Integrating In Vivo Validation, Network Pharmacology and Molecular Dynamics Simulation

Marium Abdul Majeed[1], Rimsha Shamshad[1], Muhammad Shoaib Mehboob[2], Sammar Mushyat[1], Muhammad Tahir[1*], Yousra[3], Hira Khurram Malik[4], Dr. Asma Yawar[5]

[1]Faculty of Life Sciences, Government College University Faisalabad, Faisalabad, Pakistan, mariumabdulmajeed293@gmail.com, rimshash215@gmail.com, sammarmushyat@gmail.com, tahirsabqi2300@gmail.com
[2]School of Built and Natural Environments, College of Science and Engineering, University of Derby, Derby, United Kingdom, shoaibmehboob43@gmail.com
[3]Faculty of Life Sciences, University of Agriculture, Faisalabad, Pakistan, yusranasir1611@gmail.com
[4]Department of Pharmacology, Faculty of Pharmacology, The University of Lahore, Pakistan, drhirakhurrammalik@gmail.com
[5]Department of Nutritional Sciences, Faculty of Science and Technology, Government College Women University Faisalabad, Pakistan, Asmabukhari758@gmail.com
[*]Corresponding author: Muhammad Tahir (tahirsabqi2300@gmail.com)

ABSTRACT: **Background**: Diabetic wounds heal poorly because inflammation persists, angiogenesis is impaired and signalling becomes dysregulated, so multi-target therapies are needed. Moringa concanensis Nimmo is a traditional medicinal plant rich in flavonoids, but its wound-healing activity and mechanism have not been characterised. Diabetes was induced in male BALB/c mice with streptozotocin (200 mg/kg, i.p.). Full-thickness 5 mm excision wounds were then left untreated or treated topically with silver sulfadiazine or 50% (w/w) hydroethanolic M. concanensis leaf-extract ointment (n = 6 per group). Wound contraction was measured planimetrically (ImageJ), and IL-7 and IL-1β expression was quantified by RT-qPCR. Phytocompounds were screened for drug-likeness (SwissADME), mapped to predicted targets (SwissTargetPrediction) and intersected with diabetic-wound genes (GeneCards). Hub genes were ranked by protein–protein interaction topology (STRING, cytoHubba DMNC) and annotated by GO/KEGG enrichment. The lead interaction was examined by docking (AutoDock Vina) and by 100 ns molecular dynamics (Desmond). All statistics were computed in Python with one-way ANOVA and Tukey HSD or Welch tests with Holm correction. On day 3, M. concanensis produced greater wound contraction than the untreated diabetic control (46% vs 27%; mean difference 19 percentage points, 95% CI 4.7 to 33.3; Tukey $p = .009$; $d = 2.00$). The difference on day 5 was of similar size but less precise (16 points, $p = .093$). The extract-treated wounds healed at 12.0% per day, compared with 9.25% per day for controls. By day 5, IL-7 expression was 2.06-fold higher (Holm $p < .001$) and IL-1β expression was 0.42-fold of control (Holm $p = .014$). Of 14 phytocompounds, 13 satisfied Lipinski's rule. These compounds shared 382 targets with the disease set, and IL7, AKT1 and STAT3 ranked among the top DMNC hubs. Kaempferol bound IL-7 at −6.5 kcal/mol, and the

Natural Resources for Human Health
eISSN: 2583-1194

complex stayed stable over 100 ns (ligand RMSD about 2.8 Å; PC1 = 48.3% of motion). M. concanensis accelerates early diabetic wound closure and shifts the cytokine milieu towards resolution. The data point to IL-7–linked JAK–STAT/PI3K–Akt signalling as a plausible, testable mechanism.

Highlights

- Treated wounds showed a time-dependent rise in IL-7 and a fall in IL-1β transcripts relative to GAPDH.
- Network pharmacology of 14 drug-like phytocompounds placed IL7, AKT1 and STAT3 among the top DMNC-ranked hub genes, with PI3K–Akt as the most recurrent pathway.
- Kaempferol docked to IL-7 (−6.5 kcal/mol) and remained in the binding site throughout a 100 ns molecular dynamics simulation.
- All statistics were re-run in an open Python pipeline, with effect sizes, 95% confidence intervals and correction for multiple comparisons.

Abstract

Keywords:

1. INTRODUCTION

In 2021, there were an estimated 537 million adults with diabetes globally; this is expected to reach 783 million by 2045 (Ashraf et al., 2025; Sun et al., 2022). Major and expensive complications include diabetic foot ulcers and other chronic diabetic wounds. They happen often and are a precursor to the majority of non-traumatic lower-limb amputations (Afzal et al., 2025; Armstrong et al., 2017; Armstrong et al., 2023; Boulton et al., 2005). Most ulcers fail to heal even with offloading, debridement, infection control and advanced dressings for several months. This ongoing unmet need has led to a need to look at the possibility of developing an economical multi-targeted agent (Armstrong et al., 2023).

The repair process is normal, involving a series of overlapping stages including haemostasis, inflammation, proliferation and remodelling (Guo & DiPietro, 2010; Gurtner et al., 2008). Chronic hyperglycaemia has a negative effect on each stage of diabetes (Shahzadi et al., 2025). Advanced glycation end-products and oxidative stress build up (Deng et al., 2021; Singh et al., 2014), macrophages stay in a pro-inflammatory state and signalling through IL-1β is continuous (Dinarello, 2018; Eming et al., 2007). Impaired angiogenesis (Okonkwo and DiPietro, 2017), defective fibroblast and keratinocyte migration and matrix deposition (Brem and Tomic-Canic, 2007; Falanga, 2005; Loots et al., 1998; Martin and Nunan, 2015). These defects are interrelated with each other and hence, the clinical success has been limited with the use of single-target agents. This means that multi-component phytotherapies with pleiotropic actions are also logical alternatives (Burgess et al., 2021).

The genus Moringa (Moringaceae) has a long ethnomedical history. The leaves of Moringa oleifera are rich in quercetin and kaempferol glycosides, chlorogenic acid, other phenolics which possess antioxidant, anti-inflammatory and antidiabetic properties (Anwar et al., 2007; Leone et al., 2015; Vergara-Jimenez et al., 2017). An aqueous fraction of M. oleifera leaves was seen to promote wound healing in diabetic rats (Amali Muhammad et al., 2016). Moringa concanensis Nimmo is another species which is less studied and is used traditionally in the dry regions of the Indian sub continent for treating diabetes, inflammation and skin disorders. The leaves of this plant have flavonoids, phenolics, terpenoids and sterols that have measurable antioxidant activity (Singh et al., 2019; Singh et al., 2024). Nevertheless, its wound healing activity in diabetes has never been evaluated in an experimental setting and the molecular targets are yet to be determined.

Network pharmacology provides a systems-level approach to mapping out the multitude of components in a botanical extract to disease-relevant protein networks (Hopkins, 2008; Li & Zhang, 2013; Zhao et al., 2024). In addition to molecular docking, molecular dynamics (MD) simulation can also be used to deduce mechanistic hypotheses that can be tested in vivo. Interleukin-7 (IL-7) stands out among the candidate mediators. It is produced by keratinocytes (Heufler et al., 1993), it signals through the IL-7Rα/γc to activate JAK–STAT and PI3K–Akt cascades (Mazzucchelli & Durum, 2007; Mackall et al., 2011), and it has been linked to keratinocyte migration and to healing chronic wounds (Bartlett et al., 2016). The compound

kaempferol, which is rich in Moringa, has been found to have a beneficial effect on diabetic wound repair on its own (Calderón-Montaño et al., 2011; Özay et al., 2019).

The aims of this study therefore were: (i) to quantify the wound healing effect of the topical M. concanensis ointment against untreated and silver sulfadiazine (SSD) treated diabetic mice; (ii) to measure the effect on the expression levels of IL-7 and IL-1β; and (iii) to identify through network pharmacology, docking and 100 ns MD simulation, the most likely interactions between phytocompounds and targets responsible for these effects. All statistical analyses were re-implemented in an open python workflow reporting effect sizes, confidence intervals, and p values along with p values, to support reproducibility.

2. MATERIALS AND METHODS

2.1. Ethics statement and study design

The study was approved by the Animal Ethics Committee of Directorate of Medical Sciences, Government College University Faisalabad (Approval No GCUF/ERB/2023/047). This work was performed in the Health Biotechnology Laboratory, GCUF, Pakistan. The reporting is done according to the ARRIVE 2.0 guidelines (Kilkenny et al., 2010, Percie du Sert et al., 2020). The workflow fundamentally involved in vivo excision wound model, transcript analysis, network pharmacology and docking and MD simulation.

2.2. Plant material and ointment preparation

Fresh leaves of M. concanensis were taken from the Ayub Agricultural Research Institute (AARI), Faisalabad. They were washed in distilled water, shade dried and ground to a fine powder. The powder (1 g/100 mL) was macerated overnight at room temperature with 50% ethanol and some shaking in between, filtered through Whatman No. 1 paper and concentrated down under reduced pressure on a rotary evaporator. The semisolid crude extract was mixed in 1:1 (w/w) ratio with petroleum jelly and prepared an ointment of 50% (w/w) standardisation. This was homogenised under sterile conditions, and stored in air-tight containers at 4 °C until use (Figure 3).

2.3. Animals, induction of diabetes and wounding

Male BALB/c mice (adult) were maintained under controlled temperature and 12 h light/dark cycle with standard chow and water ad libitum and acclimatised prior to experimentation (Figure 1A–B). After a 12 h fast, diabetes was induced with a single intraperitoneal injection of freshly prepared STZ (200 mg/kg) in chilled 0.1 M sodium citrate buffer (pH 4.5) (Furman, 2021). Fasting blood glucose was taken from the tail vein using a digital glucometer and mice with blood glucose levels > 180 mg/dL were included in the study. The dorsal skin was shaved and disinfected with 70% ethanol under ketamine–xylazine anaesthetic. Using a sterile biopsy punch (Figure 1C–D), full-thickness excision wounds of 5 mm diameter were made through the epidermis, dermis, and subcutis.Full-thickness, 5 mm diameter, excision wounds were created using a sterile biopsy punch (Galiano et al., 2004; Rhea & Dunnwald, 2020) (Figure 1C–D). Animals were isolated post surgery.

2.4. Group allocation and treatment

Diabetic mice were randomly divided into three groups (6 mice each). Group A (diabetic control) was not treated topically. Group B (standard) was treated with 1% silver sulfadiazine ointment. M. concanensis ointment was given at 50% (w/w) to group C. Two dorsal injuries were given to each mouse. In groups B and C one wound was treated and the other wound on the same animal was untreated and served as a within-animal control, while the treated wound served for between-group comparisons. The treatments were twice daily and were applied under sterile conditions. The appearance of the wounds was observed daily and photographs were taken at day 0, day 1, day 3 and day 5 of the experiment under constant illumination and at a fixed camera distance (Figures 2 and 4).

2.5. Wound contraction

Wound area was measured in ImageJ (Schneider et al., 2012). Percentage wound contraction on day t was calculated as $[(A_0 - A_t)/A_0] \times 100$, where A_0 is the initial wound area and A_t the area on day t.

2.6. RNA extraction, cDNA synthesis and RT-qPCR

The total RNA was extracted using FavorPrep™ blood/tissue total RNA kit following the manufacturer's instructions. The integrity of rRNA was evaluated by separating on agarose gels (28S and 18S rRNA bands) (Figure 7A). To prepare cDNA,

oligo(dT) primers and RevertAid reverse transcriptase were used, and, following the instructions on the kit, 0.1 ng–5 μg of RNA was used as a template. The levels of IL-6, TNF-α, IL-1β and GAPDH were confirmed by end-point RT-PCR (Figure 7B–C). The transcripts of IL-7 and IL-1β were then quantified on days 0, 1, 3 and 5 and normalised to GAPDH and expressed as fold change using the 2−ΔΔCt method (Livak & Schmittgen, 2001).

2.7. Phytochemical selection and drug-likeness

The phytoconstituents reported for Moringa leaves, bark and seeds (Leone et al., 2015; Singh et al., 2019; Vergara-Jimenez et al., 2017) were downloaded from PubChem and submitted to SwissADME (Daina et al., 2017) for the evaluation of molecular weight (MW), hydrogen-bond donors (HBD), hydrogen-bond acceptors (HBA), consensus log Po/w and rotatable bonds. At most 1 violation of Lipinski's rule of five (Lipinski et al., 2001) was allowed. The leaves of Moringa were found to contain 14 compounds for target prediction (Table 4), which were kept as a reference set of glycosides, since 3 of the criteria were not met by rutin.Rutin was kept as a reference glycoside, since it violated 3 criteria and was a dominant flavonol in Moringa leaves, which gave 14 compounds for target prediction (Table 4).

2.8. Target prediction and disease-gene mining

The targets for each of the 14 compounds were predicted using SwissTargetPrediction (Daina et al., 2019) (Homo sapiens) and only the targets that had a probability > 0.7 were kept, resulting in 436 unique proteins. To identify diabetic wound-healing genes, we used the GeneCards (Stelzer et al., 2016) database and retrieved the genes with the following query terms: diabetic wound, diabetic foot ulcer, chronic diabetic wound, and delayed wound healing in diabetes. Gene symbols were harmonised with UniProt and the Intersection was calculated using InteractiVenn (Heberle et al., 2015).

2.9. PPI network, hub genes and enrichment

Targets were overlapping and uploaded on STRING (Szklarczyk et al., 2023) (H. sapiens) to create a protein–protein interaction (PPI) network. The network was imported into Cytoscape 3.9.1 (Shannon et al., 2003) and "hub" genes were ranked using the DMNC (density of maximum neighbourhood component) algorithm in cytoHubba (Chin et al., 2014). GO biological process, molecular function and KEGG enrichment were performed in ShinyGO v0.82 (Ge et al., 2020) using the false discovery rate (FDR) < 0.05.

2.10. Molecular docking

The crystal structure of human IL-7 (PDB ID 3DI2) was prepared by removing water and heteroatoms, adding polar hydrogens and assigning charges. The 3D structures of the ligands were downloaded from PubChem and then energy-minimized and converted to PDBQT format using Open Babel (O Boyle et al., 2011). Docking has been performed with AutoDock Vina (Trott & Olson, 2010) in PyRx 0.8 (Dallakyan & Olson, 2015) with the use of a grid box centered on the predicted binding pocket. The hydrogen-bond, π and hydrophobic contacts for the lowest energy pose were investigated.

2.11. Molecular dynamics simulation

The IL-7–kaempferol complex has been simulated for 100 ns in Desmond 2024-1 (Schrödinger 2024-1) (Bowers et al., 2006). The complex was solvated into an orthorhombic TIP3P water box (Jorgensen et al., 1983), neutralised with counter-ions and then adjusted to contain 0.15 M NaCl prior to energy minimisation using the OPLS4 force field (Lu et al., 2021). Prior to the production run it was equilibrated in the NVT and NPT ensembles (300 K, 1 atm) and frames were saved every 100 ps over the course of the equilibration run. The backbone and ligand RMSD and the per-residue RMSF and principal component analysis (PCA) of Cα coordinates were performed.

2.12. Statistical analysis

Data are reported as means ± SEM (n = 6/group). All inferential statistics were performed using Python 3 (NumPy, pandas, SciPy, Matplotlib) and as Supplementary Code S1, a scripted and version controlled pipeline was provided. Group summary statistics (mean, SEM, n) were used to compute tests, which use exact closed-form ANOVA, Tukey and Welch formulae. Animal-level data can be directly entered into the script for re-analysis. One-way ANOVA and Tukey's honestly significant difference (HSD) test (Tukey, 1949) based on the studentised range distribution were used to compare the wound contraction on each day among the three groups. To each comparison, we add the mean difference (and its simultaneous 95% CI), Cohen's d (standardised by the root mean-square error) as well as the η^2 for the ANOVA. Healing rate was calculated as the

least-squares slope of the mean contraction with time (days 1–5). Data for gene expression in treated and control mice were compared on each day using the Welch's t-test. Hedges' g was computed and the p values adjusted across 4 time points for each gene using Holm–Bonferroni method. Hypergeometric distribution was used to test for over-representation of compound targets in the disease set using a background of 20,000 human protein-coding genes. The correlation between the DMNC score with the membership to any given pathway was determined using Spearman's ϱ. Two-sided α was 0.05.

3. RESULTS

3.1. Diabetic model and wound creation

All the mice injected with STZ that were enrolled had fasting blood glucose levels >180 mg/dL. The full thickness wound on the dorsum was standardised (Figure 1) with treatments as described (Figure 2). The plant of M. concanensis and 50% (w/w) ointment are depicted in Figure 3.



Figure 1. Experimental housing, dorsal preparation and creation of excision wounds. (A) Standard housing and acclimatisation; (B) handling of a BALB/c mouse; (C) dorsal shaving and disinfection with 70% ethanol; (D) full-thickness 5 mm excision wound created with a sterile biopsy punch.

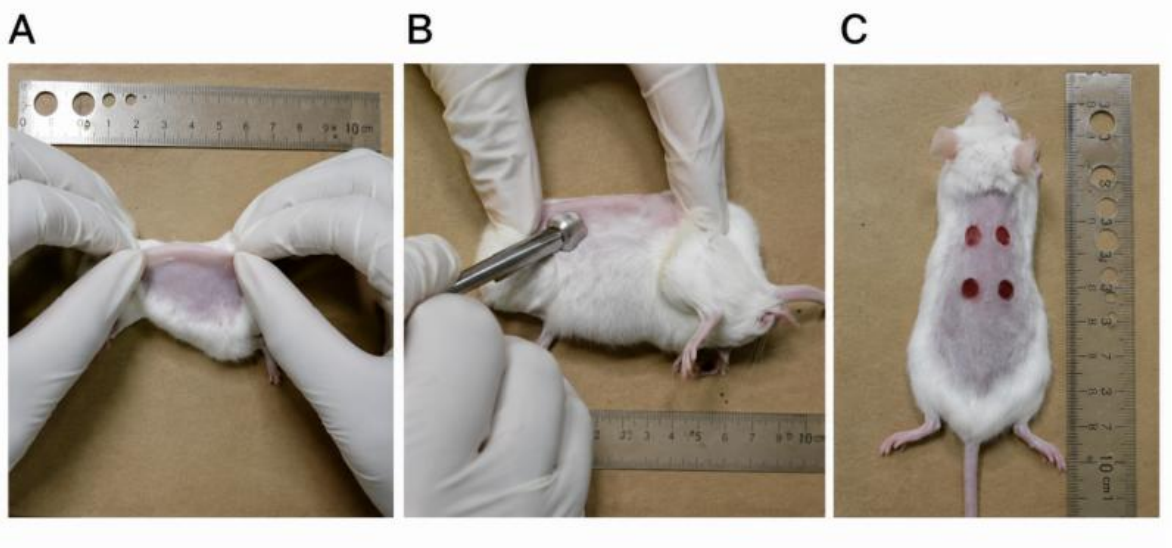

Figure 2. Group allocation and topical treatment. (A) Dorsal bilateral wound model in a diabetic BALB/c mouse; (B) application of silver sulfadiazine ointment; (C) application of 50% (w/w) *M. concanensis* ointment.

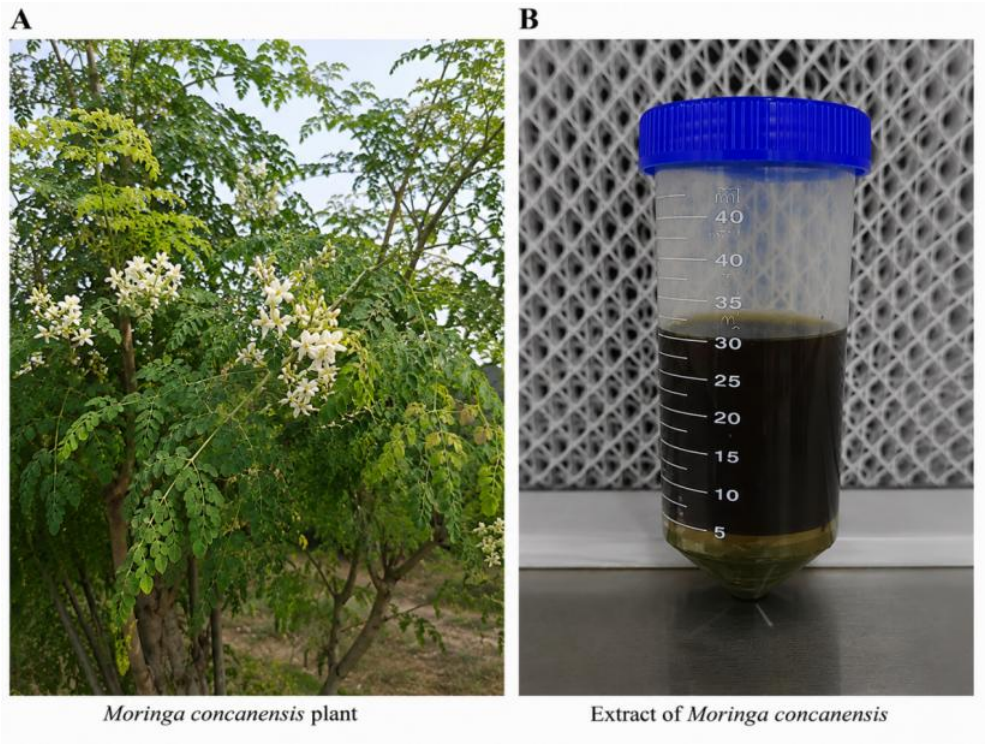

Figure 3. Preparation of the *M. concanensis* formulation. (A) Plant material collected for extraction; (B) hydroethanolic crude extract incorporated into petroleum jelly as a 50% (w/w) ointment.

3.2. *M. concanensis* accelerates wound contraction

All the groups exhibited the wound area reducing over the days, most prominently in M. concanensis-treated wounds on days 3 and 5 (Figure 4).

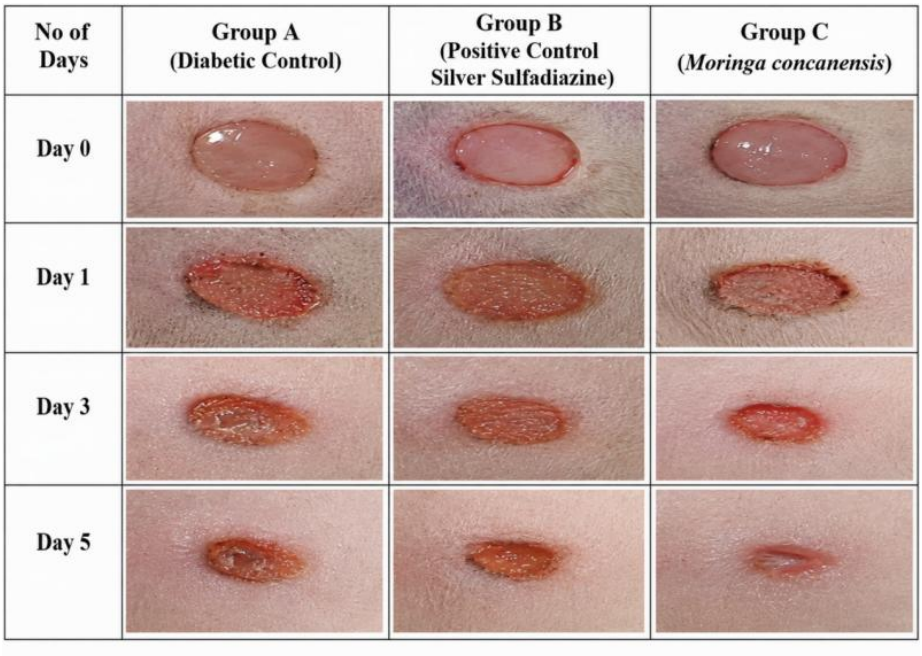

Figure 4. Macroscopic progression of diabetic wounds on days 0, 1, 3 and 5 in group A (untreated diabetic control), group B (silver sulfadiazine) and group C (50% w/w *M. concanensis*).

The contracting of the time was also found to be greater in all the groups with M. concanensis the most consistently contracting group (Figure 5; Table 1). On day 1, the groups did not differ ($F(2, 15) = 1.85$, $p = .191$). By day 3, the treatment effect was significant ($F(2, 15) = 6.12$, $p = .011$, $\eta^2 = 0.45$). The M. concanensis wounds healed 19 percentage points more than the diabetic wounds that had not been treated with M. concanensis (95% CI 4.7 to 33.3; $p = .009$; $d = 2.00$). There was no significant difference between the control group (12 points) and the SSD group ($p = .106$, Fig. 6; Tab. 2) and no significant difference between M. concanensis and SSD ($p = .430$, Fig. 6; Tab. 2). The effect of M. concanensis was similar to the control on day 5 (16 points; $d = 1.31$). However, between-animal variance was larger (pooled SD ≈ 12.2 points), so the omnibus test ($F(2, 15) = 2.57$, $p = .109$) and the pairwise contrast (95% CI -2.4 to 34.4; $p = .093$) did not reach significance. The mean healing rates per day for each of the days 1-5 were 12.0% for M. concanensis, 10.75% for SSD and 9.25% for no treatment. The extract thus resulted in an approximately 30% higher closure rate in comparison to the non-treated diabetic wounds.

Table 1. Wound contraction (%) in streptozotocin-diabetic mice and one-way ANOVA by day.

Day	Diabetic control	Silver sulfadiazine	*M. concanensis*	F(2, 15)	p	η^2
Day 1	12 ± 2.0	15 ± 1.5	17 ± 2.0	1.85	.191	0.20
Day 3	27 ± 3.0	39 ± 4.0	46 ± 4.5	6.12	.011	0.45
Day 5	49 ± 5.0	58 ± 5.0	65 ± 5.0	2.57	.109	0.26

Values are mean ± SEM, n = 6 per group. η^2, proportion of variance explained by treatment. Source: Supplementary Code S1.

Table 2. Tukey HSD pairwise comparisons of wound contraction.

Day	Contrast	Δ mean (% points)	95% CI (simultaneous)	q	p (Tukey)	Cohen's *d*
Day 1	*M. concanensis* − Control	5.0	-1.8 to 11.8	2.71	.169	1.10
Day 1	*M. concanensis* − SSD	2.0	-4.8 to 8.8	1.08	.729	0.44
Day 1	SSD − Control	3.0	-3.8 to 9.8	1.62	.501	0.66
Day 3	*M. concanensis* − Control	19.0	4.7 to 33.3	4.89	.009	2.00
Day 3	*M. concanensis* − SSD	7.0	-7.3 to 21.3	1.80	.430	0.74
Day 3	SSD − Control	12.0	-2.3 to 26.3	3.09	.106	1.26
Day 5	*M. concanensis* − Control	16.0	-2.4 to 34.4	3.20	.093	1.31
Day 5	*M. concanensis* − SSD	7.0	-11.4 to 25.4	1.40	.594	0.57
Day 5	SSD − Control	9.0	-9.4 to 27.4	1.80	.431	0.73

SSD, silver sulfadiazine. Δ mean, difference in mean wound contraction; q, studentised range statistic (k = 3, df = 15).

Natural Resources for Human Health
eISSN: 2583-1194

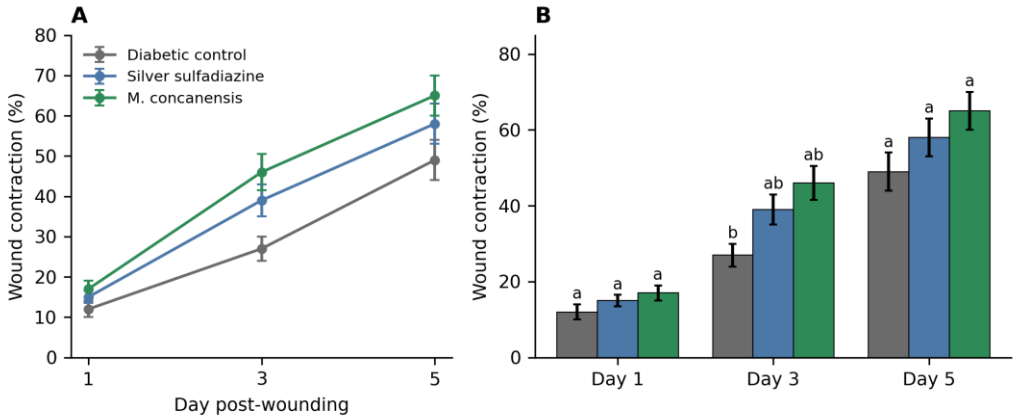

Figure 5. Quantitative wound contraction. (A) Time course of mean ± SEM contraction (n = 6 per group). (B) Contraction by day; bars that share a letter within a day do not differ (Tukey HSD, α = 0.05).

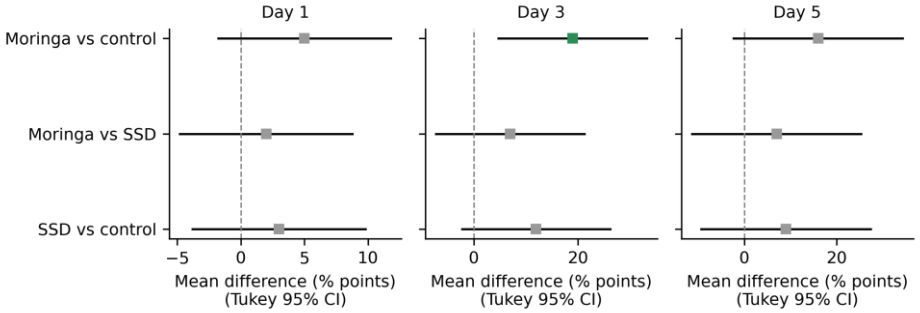

Figure 6. Effect estimates for wound contraction. Tukey-adjusted mean differences (squares) with simultaneous 95% CIs for each pairwise contrast on days 1, 3 and 5. Green squares mark contrasts with $p < 0.05$. SSD, silver sulfadiazine.

3.3. RNA quality and cytokine expression

Both total RNA and cDNA resulted in distinct bands of 28S and 18S rRNA with no band smearing, and cDNA allowed amplification of IL-6, TNF-α, IL-1β and the GAPDH reference gene in both groups (Figure 7).

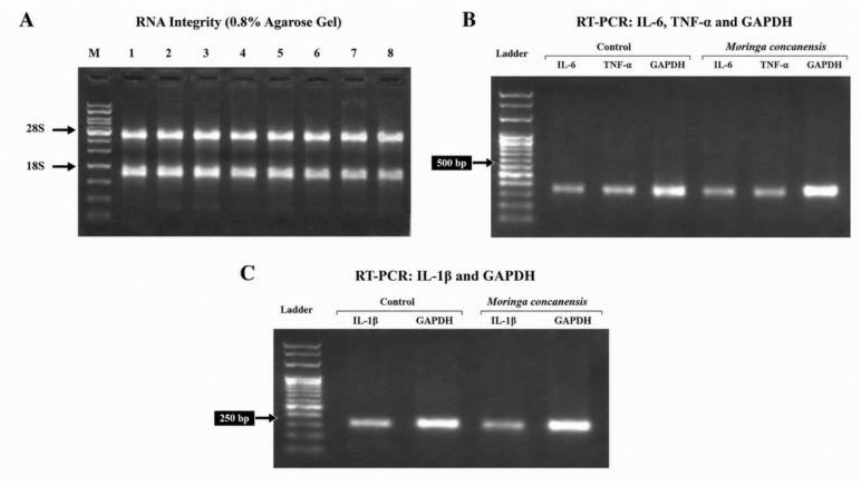

Figure 7. Validation of RNA and cDNA quality. (A) Total RNA on 0.8% agarose showing intact 28S and 18S rRNA; (B) RT-PCR amplification of IL-6 and TNF-α with GAPDH; (C) amplification of IL-1β and GAPDH in untreated diabetic and *M. concanensis*-treated mice.

The expression of IL-7 increased gradually in treated mice and was significantly increased compared to control mice from day 1 (Figure 8A; Table 3). The fold differences were 1.93 on day 1 (Holm p = .043), 1.88 on day 3 (Holm p < .001) and 2.06 on day 5 (Holm p < .001; Hedges' g = 4.40). There was no difference between the groups at baseline (p = .297). The treated mice showed a fourfold increase (4.5-fold) in IL-7 levels compared to the control mice and over the level measured on day 0 for each group. There was also a decrease in the expression of IL-1β in both groups over time, and a larger decrease when treated (Figure 8B). Treated values were 0.71, 0.56 and 0.42 times control values on days 1, 3 and 5 (Holm p = .007, = .003 and = .014; day 5 g = -1.86). Additionally, there was a slight decrease in baseline IL-1β in mice treated (p = .018) and this was adjusted for day 0 as a sensitivity check. When M. concanensis was used, Expression decreased to 19% of baseline, when it was not used, Expression decreased to 39% of baseline, showing that the larger decrease was not only due to the baseline imbalance.

Table 3. Relative expression of IL-7 and IL-1β (normalised to GAPDH) in untreated and *M. concanensis*-treated diabetic wounds.

Gene	Day	Control	Treated	Treated/Control	Welch t (df)	p	p (Holm)	Hedges' *g*
IL-7	Day 0	1.10	1.50	1.36	1.11 (8.7)	.297	.297	0.59
IL-7	Day 1	1.40	2.70	1.93	2.91 (7.4)	.022	.043	1.55
IL-7	Day 3	2.50	4.70	1.88	6.10 (8.7)	< .001	< .001	3.25
IL-7	Day 5	3.30	6.80	2.06	8.25 (10.0)	< .001	< .001	4.40
IL-1β	Day 0	1.35	1.15	0.85	-2.83 (10.0)	.018	.018	-1.51
IL-1β	Day 1	1.10	0.78	0.71	-4.10 (9.7)	.002	.007	-2.18
IL-1β	Day 3	0.85	0.48	0.56	-4.74 (9.7)	< .001	.003	-2.52
IL-1β	Day 5	0.52	0.22	0.42	-3.49 (9.0)	.007	.014	-1.86

Values are mean relative expression ($2^{-\Delta\Delta Ct}$), n = 6 per group. Holm correction applied across the four time points of each gene.

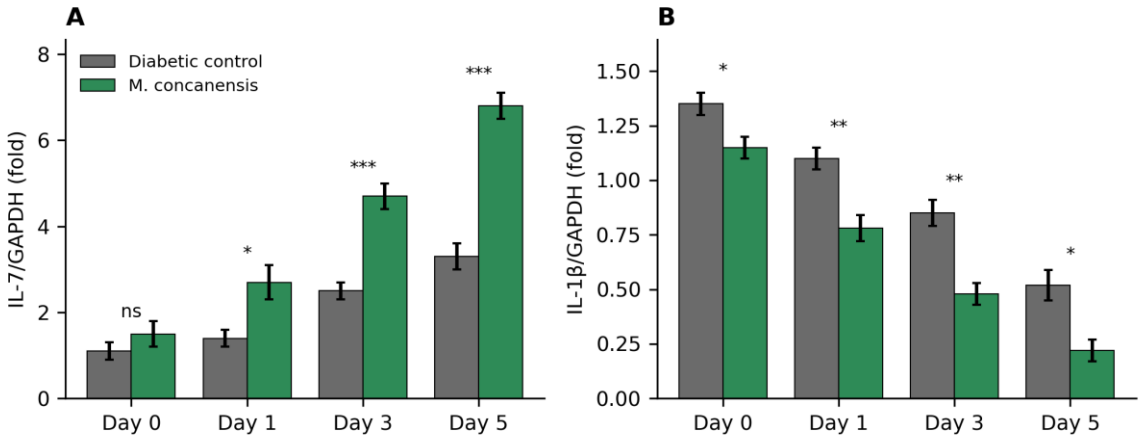

Figure 8. Cytokine transcript dynamics. (A) IL-7 and (B) IL-1β relative to GAPDH in untreated diabetic (grey) and *M. concanensis*-treated (green) mice. Bars show mean ± SEM (n = 6). One, two and three asterisks denote p < 0.05, < 0.01 and < 0.001; ns, not significant (Welch *t*-test, Holm-adjusted).

3.4. Drug-likeness of *M. concanensis* phytoconstituents

Out of the 14 phytocompounds that were assessed, 11 did not have a violation of the Lipinski rule. Chlorogenic acid (610.5 g/mol, 10 HBD, 16 HBA), and rutin (six hydrogen-bond donors) and myricetin (six hydrogen-bond donors) each had one violation; however, rutin had three violations (MW 610.5 g/mol, 10 HBD, 16 HBA) (Table 4; Figure 9). The mean MW of the compounds was 289.57 g/mol, and the mean log Po/w of all the compounds was 1.62 (excluding rutin). All compounds had ≤ 10 rotatable bonds. So 13 of 14 compounds conformed to the rule of five and rutin was progressed as a reference glycoside (Section 2.7).

Table 4. Physicochemical properties and Lipinski rule-of-five assessment of *M. concanensis* phytoconstituents (SwissADME).

Compound	MW (g/mol)	HBD	HBA	Log $P_{o/w}$	Rot. bonds	Violations	Drug-like (≤ 1)
Quercetin	302.23	5	7	1.63	1	0	Yes
Kaempferol	286.24	4	6	1.70	1	0	Yes
Rutin	610.52	10	16	−1.12	6	3	No
Chlorogenic acid	354.31	6	9	0.87	5	1	Yes
Caffeic acid	180.16	3	4	0.97	2	0	Yes
Gallic acid	170.12	4	5	0.21	1	0	Yes
Ferulic acid	194.18	2	4	1.42	3	0	Yes
β-Sitosterol	414.71	1	1	4.73	6	0	Yes
Moringinine	209.28	2	3	1.84	4	0	Yes
Apigenin	270.24	3	5	1.89	1	0	Yes
Isorhamnetin	316.26	4	7	2.35	2	0	Yes
Myricetin	318.23	6	8	1.08	1	1	Yes
Linalool	154.25	1	1	2.70	4	0	Yes
Eugenol	164.20	1	2	2.37	3	0	Yes

Lipinski thresholds: MW ≤ 500, HBD ≤ 5, HBA ≤ 10, log P ≤ 5. Violation counts were recomputed in Python from the tabulated descriptors.

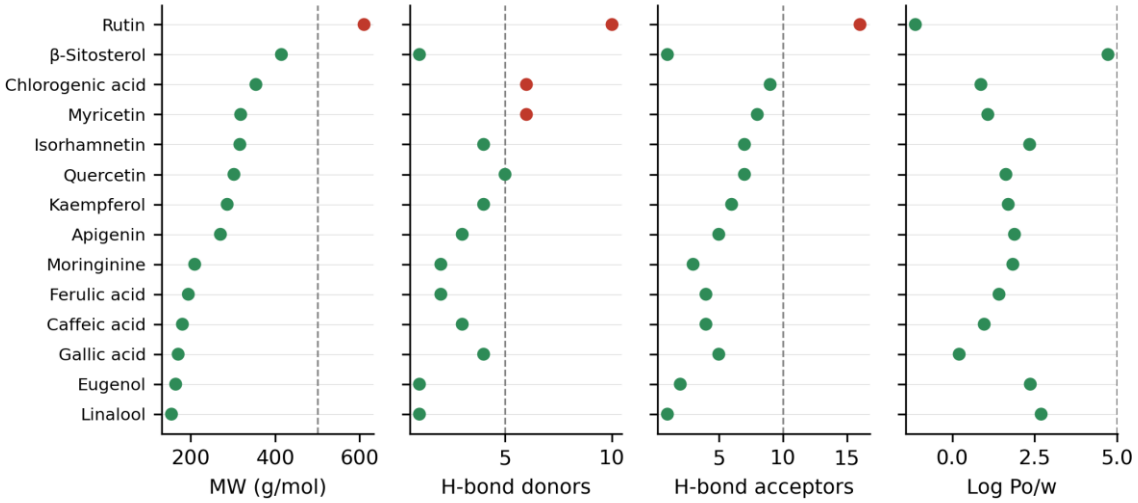

Figure 9. Drug-likeness map. Each compound is plotted against the four Lipinski descriptors; dashed lines mark the rule-of-five thresholds, and red points exceed a threshold.

3.5. Shared targets, PPI network and hub genes

SwissTargetPrediction identified 436 high-confidence targets (probability >0.7) in the 14 compounds and GeneCards retrieved 18,246 genes related to diabetes wound. There were 382 targets at the intersection, accounting for 87.6% of the compound targets (Figure 10). This overlap is not significant, and is not greater than that expected by chance (expected = 398; fold enrichment = 0.96; hypergeometric p = .996). Hence, the intersection was considered as a permissive filter and the prioritisation was done based on network topology and enrichment.

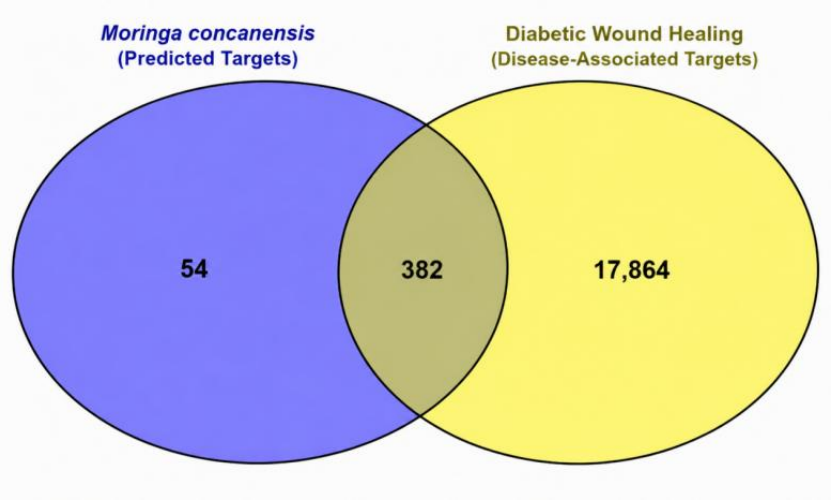

Figure 10. Venn diagram of the 436 predicted *M. concanensis* targets and the 18,246 diabetic wound-related genes, with 382 shared targets.

The 382 common targets were used to construct a STRING network (Figure 11). According to cytoHubba, ten genes were ranked as hub genes in DMNC namely AKT1, STAT3, IL7, EGFR, TNF, IL1B, VEGFA, PTGS2, HSP90AA1 and SRC. Their scores were tightly clustered (mean 0.879 ± 0.031; range 0.833–0.929) (Table 5; Figure 12A). The DMNC score was not significantly correlated with the number of KEGG pathways that were mapped to each hub (Spearman ϱ = 0.61, p = .059).

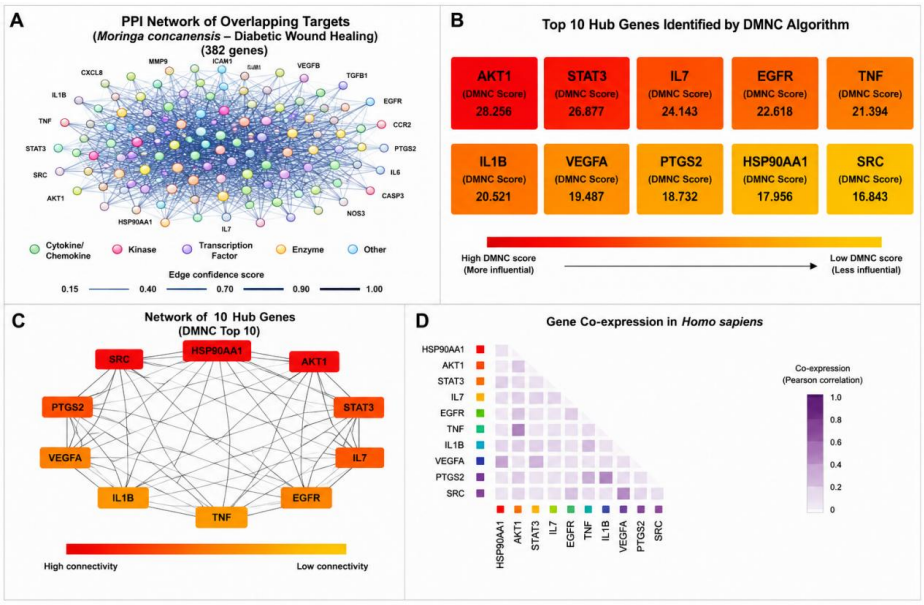

Figure 11. Network pharmacology of *M. concanensis* targets in diabetic wound healing. (A) STRING protein–protein interaction network of the shared targets; (B) Cytoscape visualisation with the top ten DMNC-ranked hub genes highlighted.

Table 5. Top ten hub genes ranked by DMNC and their principal KEGG pathways.

Gene	DMNC score	No. of pathways	Representative KEGG pathways
AKT1	0.9288	10	PI3K–Akt; AGE–RAGE; HIF-1; MAPK; VEGF; FoxO; focal adhesion; insulin resistance
STAT3	0.9155	9	JAK–STAT; PI3K–Akt; HIF-1; cytokine–cytokine receptor; chemokine; AGE–RAGE; Th17 differentiation
IL7	0.9018	6	JAK–STAT; cytokine–cytokine receptor; PI3K–Akt; T-cell receptor
EGFR	0.8962	7	EGFR-TKI resistance; PI3K–Akt; MAPK; ErbB; focal adhesion; actin cytoskeleton
TNF	0.8842	7	TNF; NF-κB; cytokine–cytokine receptor; AGE–RAGE; apoptosis; MAPK
IL1B	0.8726	6	IL-17; TNF; cytokine–cytokine receptor; NF-κB
VEGFA	0.8615	6	VEGF; HIF-1; PI3K–Akt; focal adhesion; ECM–receptor interaction
PTGS2	0.8549	6	TNF; IL-17; VEGF; NF-κB; lipid and atherosclerosis
HSP90AA1	0.8463	5	PI3K–Akt; protein processing in ER; AGE–RAGE; estrogen
SRC	0.8326	7	focal adhesion; chemokine; actin cytoskeleton; VEGF; MAPK; endocytosis

Pathway recurrence analysis of the hubs revealed that 6 out of the 10 genes shared the PI3K–Akt signalling pathway. AGE–RAGE signalling in diabetic complications, MAPK, VEGF, focal adhesion and cytokine–cytokine receptor interactions were each common to four, and HIF-1 to three (Figure 12B). The full GO and KEGG enrichment profile of the hub genes is shown in Figure 13. The recurrent pathways include inflammatory pathways (TNF, NF-κB, IL-17, JAK–STAT), cell survival and growth (PI3K–Akt, MAPK, ErbB) and angiogenesis (VEGF, HIF-1) that are linked to inflammatory, proliferative and angiogenic phases of repair, respectively.

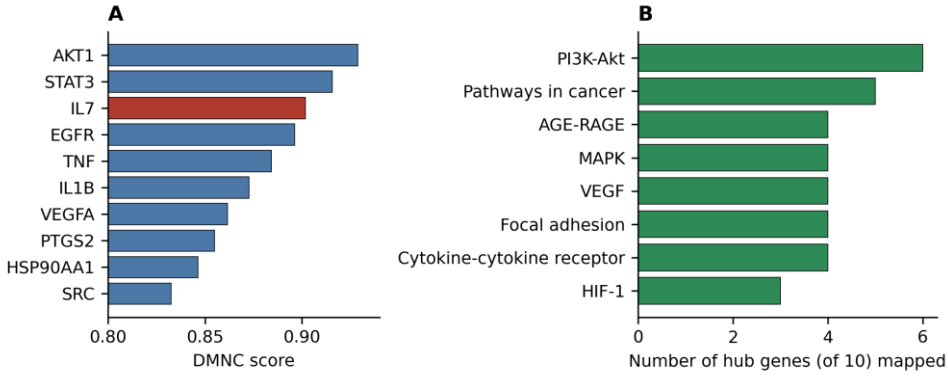

Figure 12. Hub-gene prioritisation. (A) DMNC scores of the ten hub genes (IL7 highlighted). (B) Number of hub genes mapped to each of the most recurrent KEGG pathways.

Natural Resources for Human Health
eISSN: 2583-1194

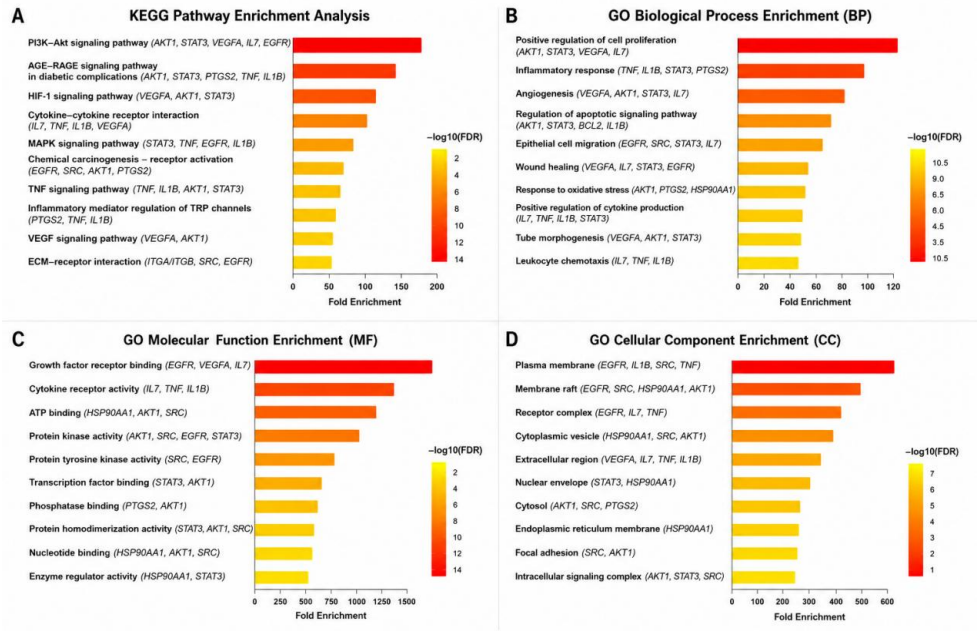

Figure 13. GO and KEGG enrichment of the ten hub genes (ShinyGO v0.82). (A) KEGG pathways; (B) GO biological process; (C) GO molecular function; (D) GO cellular component.

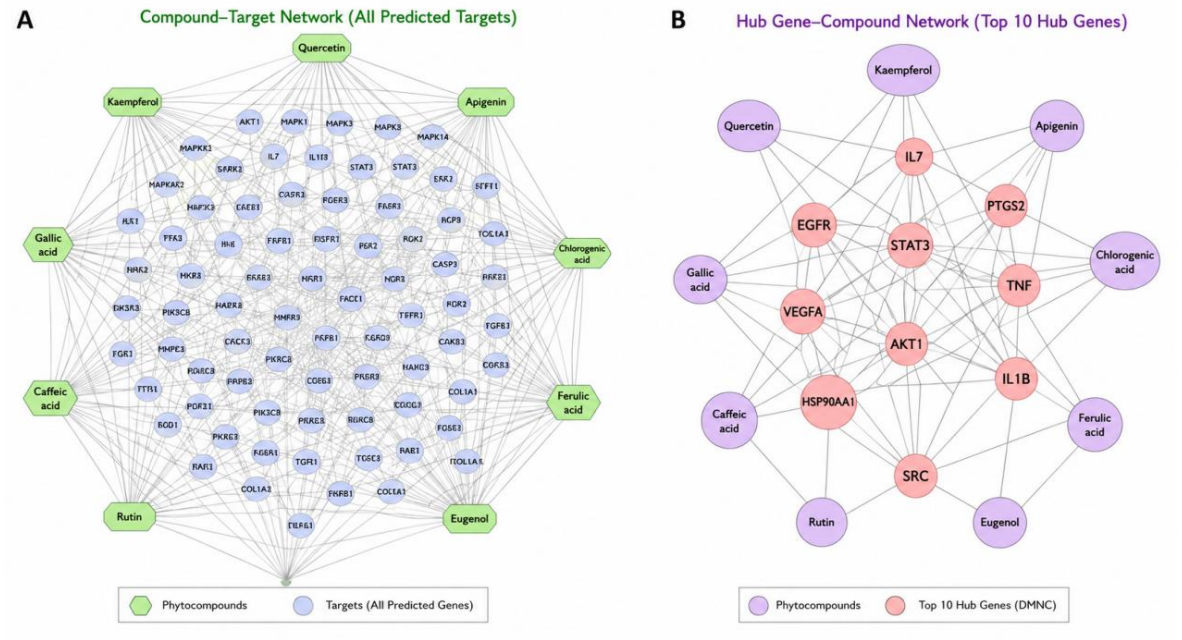

Figure 14. Compound–target–pathway networks linking *M. concanensis* phytocompounds to the shared diabetic wound targets and the enriched pathways.

3.6. Docking and molecular dynamics of the IL-7–kaempferol complex

Docking and molecular dynamics of IL-7–kaempferol complex are studied. Three criteria were used to select IL7 for structural analysis: it was a top three DMNC hub; it links to both the JAK–STAT and PI3K–Akt pathways; it was the transcript most strongly induced following treatment in vivo. The binding affinity of kaempferol was −6.5 kcal/mol and it docked into the pocket of IL-7 (PDB 3DI2) with a major affliction, which is a flavonol of Moringa leaves. It formed a conventional hydrogen bond with LYS108, and was anchored by interactions with GLU199, both ARG186 and PHE196

Natural Resources for Human Health
eISSN: 2583-1194

(Figure 14A). The RMSD of the protein backbone increased up to ~ 2.5 Å to ~ 4.2 Å during a 100 ns simulation and remained stable thereafter (Figure 14C). The RMSD for the ligand converged to approximately 2.8 Å and no kaempferol was found outside the pocket. The RMSF values were all less than 1.0 Å for the majority of the residues with larger variations at the termini and loops (Figure 14B). The first principal component of PCA accounted for 48.3% of the total motion of the Cα atom, and the frames were grouped together in PC1–PC2–PC3 space, with only small drift between the beginning and end of the trajectory (Figure 15). The main computational results are tabulated below in Table 6.

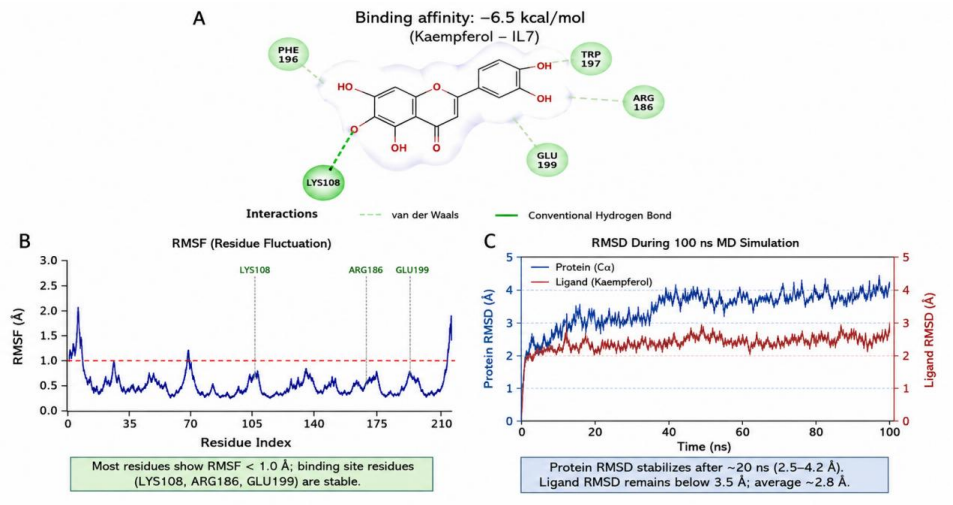

Figure 15. Structural analysis of the IL-7–kaempferol complex. (A) Docked pose (PDB 3DI2; −6.5 kcal/mol) with the hydrogen bond to LYS108 (green dashes) and the surrounding residues GLU199, ARG186, PHE196 and TRP197; (B) per-residue RMSF; (C) protein and ligand RMSD over 100 ns.

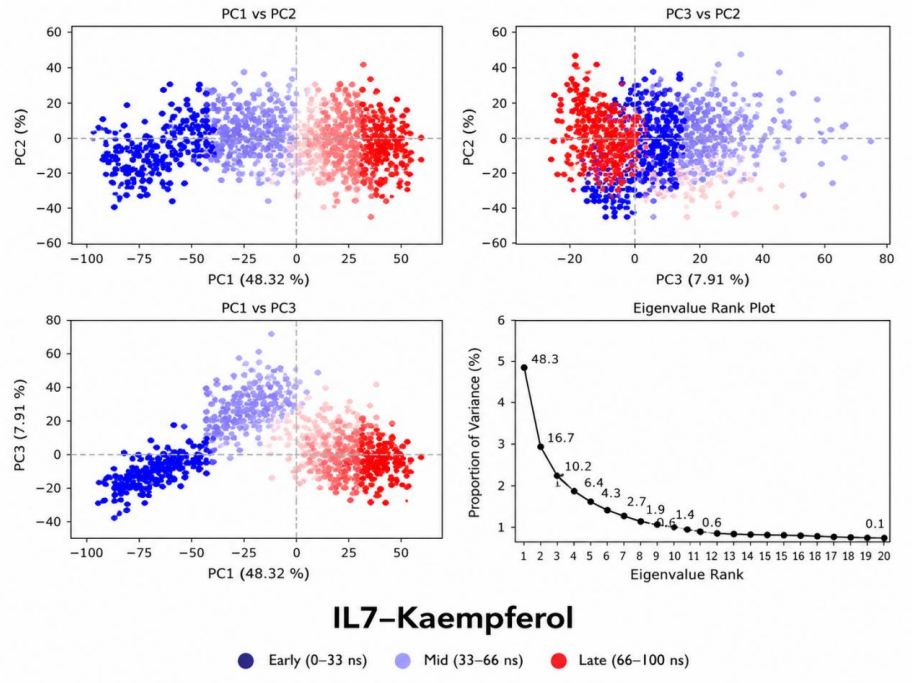

Figure 16. Principal component analysis of the 100 ns IL-7–kaempferol trajectory. Projections onto PC1–PC2, PC3–PC2 and PC1–PC3 are coloured by simulation time, and the scree plot shows that PC1 accounts for 48.3% of the variance.

Table 6. Summary of computational evidence.

Analysis	Tool	Key output
Drug-likeness	SwissADME	13/14 compounds meet Lipinski (≤ 1 violation); all ≤ 10 rotatable bonds
Target prediction	SwissTargetPrediction	436 targets (probability > 0.7)
Disease genes	GeneCards	18,246 genes; 382 shared with compound targets
Hub genes	STRING + cytoHubba (DMNC)	AKT1, STAT3, IL7, EGFR, TNF, IL1B, VEGFA, PTGS2, HSP90AA1, SRC
Pathways	ShinyGO (KEGG)	PI3K–Akt (6/10 hubs), AGE–RAGE, MAPK, VEGF, HIF-1, JAK–STAT
Docking	AutoDock Vina / PyRx	Kaempferol–IL-7: −6.5 kcal/mol; H-bond LYS108
MD (100 ns)	Desmond / OPLS4	Backbone RMSD 2.5–4.2 Å, plateau after about 20 ns; ligand RMSD about 2.8 Å; RMSF < 1 Å in the core; PC1 48.3%

4. DISCUSSION

This study is the first to show in vivo and in silico evidence of the ability of topical M. concanensis to repair diabetic wounds in an integrated fashion. The extract induced a 30% acceleration in the wound contraction rate as compared to the untreated diabetic wounds. The largest difference from control was on day 3 with d being large (d ≈ 2) and the confidence interval on d not including zero. Day 3 is a time when diabetic wounds frequently stall, a period between the inflammatory and the proliferative phase (Brem & Tomic-Canic, 2007; Eming et al., 2007; Falanga, 2005). Here, an effect focused on the concentration phase indicates that the extract has a greater effect on the escape from the inflammatory phase than just on the late remodelling phase. The mean advantage remained the same, and the range was larger, by day 5. It did not show a statistically significant benefit, and a larger, well-powered study is required to verify this finding. The results are in line with other preparations of Moringa, which have been reported as wound healing activity. An aqueous M. oleifera leaf fraction accelerated closure, re-epithelialisation and angiogenesis in diabetic rats (Amali Muhammad et al., 2016), and Moringa leaves are rich in antioxidant flavonols and phenolic acids (Leone et al., 2015; Vergara-Jimenez et al., 2017). The flavonoids and phenolics present in M. concanensis leaves are similar to that of M. sphaerocarpus, suggesting a possible common phytochemical basis (Singh et al., 2019; Singh et al., 2024). At every time point the point estimate for M. concanensis was higher than SSD, although these differences were not significant. The present data thus indicate superiority to SSD, not non-inferiority. In a molecular level, treatment resulted in two synchronized changes: a gradual increase in the production of IL-7 and a quick decrease in the production of IL-1β. Diabetic wounds have a self-sustaining inflammation that involves the central role of IL-1β (Dinarello, 2018; Eming et al., 2007). This early autumn corresponds to earlier inflammation resolution and this effect was found after correcting for the small baseline imbalance. IL-7 is produced by keratinocytes (Heufler et al., 1993), signals through the IL-7Rα/γc to activate JAK–STAT5 and PI3K–Akt (Mazzucchelli & Durum, 2007; Mackall et al., 2011), and has been associated with keratinocyte migration, and with healing chronic wounds in humans (Bartlett et al., 2016). This increase of about 2-fold of IL-7 in treated wounds on days 3-5 was correlated with the most rapid phase of contraction suggesting a role in re-epithelialisation. The network analysis arrived at the same signaling axis on its own. IL7, AKT1 and STAT3 were the three highest-ranked DMNC hubs, and PI3K–Akt was the most frequently shared pathway among the ten hubs. The remaining three nodes were inflammatory (TNF), angiogenic (VEGFA) and growth factor (EGFR, SRC), which are well-known regulators of diabetic repair and angiogenesis (Guo & DiPietro, 2010; Okonkwo & DiPietro, 2017). AGE–RAGE signalling among the recurrent pathways that were predicted to link the targets to the glycation induced damage found in diabetic tissue (Singh et al., 2014). The oxidative stress (Deng et al., 2021) is another characteristic of diabetic wounds, and the polyphenols that make up the bulk of the drug-like group have been proven to be antioxidants (Calderón-Montaño et al., 2011; Santana-Gálvez et al., 2017). This indicates that the effect of redox modulation is in addition to receptor level effects. Structural plausibility was provided for the IL-7 hypothesis by Docking and MD. Kaempferol was moderately found to bind

to IL-7 (−6.5 kcal/mol), with a hydrogen bond to LYS108. The RMSD of the ligand was less than 100 ns; the number of residues that were fluctuating was also small with the dominant motion being a single collective mode. Kaempferol has been found to have a beneficial effect on diabetic wound healing in rats (Özay et al., 2019) and our data indicate that direct target of IL-7 may be involved in this activity. Score of this magnitude would suggest interaction, but not functional modulation, so experimental proof of either kaempferol stabilisation of IL-7, alteration of its interaction with IL-7Rα or potential indirect actions via upstream transcriptional effects will be required. From a methodological perspective, two points are important. First, the overlap between the target diseases was not statistically enriched, since the wide GeneCards query retrieved most of the genome. This is a frequent phenomenon in network-pharmacology studies and is hardly reported (Hopkins, 2008; Li & Zhang, 2013). This involved prioritising based on network topology, pathway coherence and, crucially, concordance with the in vivo transcript data. Second, re-analysis of these experimental data by effect sizes, simultaneous confidence intervals and multiplicity correction has revealed where the evidence is good (day 3 contraction; IL-7 and IL-1β from day 1) and where it remains ambiguous (day 5 contraction; comparison with SSD). This transparency should enable readers to determine the level of each conclusion.

Limitations and Future Directions

There are a number of caveats that should be noted. But the sample size (n = 6 per group) was only large enough for the results at day 5 to have sufficient power, as shown in the results. (i) Follow-up was limited to 5 days and complete closure and scar quality and recurrence were not assessed. Histology (re-epithelialisation, collagen deposition, CD31+ angiogenesis) and protein level confirmation of IL-7, IL-1β and phospho-Akt/STAT3 was not carried out. (ii) The list of phytocompounds was taken from the Moringa literature and the extract did not undergo HPLC or LC–MS chemical standardisation, which means that the results presented are in silico and not measured. (iii) Independence of observations may have been affected by within-animal correlation, since both wounds were used on each animal. Model (iv) does not replicate neuropathy, ischaemia and infection of HSFUs and splinted or db/db models would be more stringent (Galiano et al., 2004; Michaels et al., 2007). (v) A docking–MD system was run without free-energy estimation (such as MM-GBSA) and without a reference ligand. Future studies should be undertaken on these points, including dose–response studies, longer follow-up, histology and immunoblotting, LC–MS fingerprinting of the extract, and functional tests, such as IL-7 neutralisation and JAK/PI3K inhibition.

CONCLUSION

The topical application of Moringa concanensis ointment treatment (50% w/w) spurred wound contraction in the STZ-diabetic mice, particularly at the early transition from inflammatory to proliferative phase and at least equaled the effect of silver sulfadiazine. Induced the expression of IL-7 and suppressed the expression of IL-1β. Both network pharmacology and docking and 100 ns MD simulation indicated the interaction of IL-7 and a stable kaempferol–IL-7 binding complex, and the IL-7/JAK–STAT/PI3K–Akt axis was proposed as potential mediators. The findings are in line with the use of M. concanensis as a candidate multi-target, low-cost adjunct for the treatment of diabetic wounds, and provide an understanding of testable mechanistic hypotheses that may be used in future preclinical and translational research.

Declarations

Ethics approval

All animal experiments were approved and followed ARRIVE 2.0 guidelines by the animal ethics committee (DMS/ERB/2023/047) of Directorate of Medical Sciences, Government College University Faisalabad (GCUF).

CRediT authorship contribution statement

Marium Abdul Majeed: Investigation, Methodology, Formal analysis, Writing – original draft. **Rimsha Shamshad:** Investigation, Data curation. **Muhammad Shoaib Mehboob:** Software, Formal analysis (computational), Writing – review & editing. **Sammar Mushyat:** Investigation, Visualisation. **Muhammad Tahir:** Conceptualisation, Supervision, Resources, Project administration. **Yousra**: Writing – review & editing. **Hira Khurram Malik**: Conceptualisation, Investigation, Data curation, Writing – review & editing

Funding

This research received no specific grant from any funding agency in the public, commercial or not-for-profit sectors.

Declaration of competing interest

The authors declare that they have no known competing financial interests or personal relationships that could have appeared to influence the work reported in this paper.

REFERENCES

[1] Afzal, M. A., Noor, M., Shahzadi, N., Saadat, S., Chaudhry, R., & Zafar, M. N. (2025). Case study of a patient with decompensated type 2 diabetes mellitus and multiple comorbidities: implications for personalised care and disease modulation. *Multidisciplinary Surgical Research Annals*, *3*(3), 744-756.

[2] Amali Muhammad, A., Fakurazi, S., Arulselvan, P., See, C. P., & Abas, F. (2016). Evaluation of wound healing properties of bioactive aqueous fraction from *Moringa oleifera* Lam on experimentally induced diabetic animal model. *Drug Design, Development and Therapy*, *10*, 1715–1728. https://doi.org/10.2147/DDDT.S96968

[3] Anwar, F., Latif, S., Ashraf, M., & Gilani, A. H. (2007). *Moringa oleifera*: A food plant with multiple medicinal uses. *Phytotherapy Research*, *21*(1), 17–25. https://doi.org/10.1002/ptr.2023

[4] Armstrong, D. G., Boulton, A. J. M., & Bus, S. A. (2017). Diabetic foot ulcers and their recurrence. *New England Journal of Medicine*, *376*(24), 2367–2375. https://doi.org/10.1056/NEJMra1615439

[5] Armstrong, D. G., Tan, T.-W., Boulton, A. J. M., & Bus, S. A. (2023). Diabetic foot ulcers: A review. *JAMA*, *330*(1), 62–75. https://doi.org/10.1001/jama.2023.10578

[6] Ashraf, M. A., Afzal, M. A., Ijaz, M., Arshad, A., Zafar, M. N., Ukkasha, S. M., & Zahid, I. (2025). Financial impact of nutrition on non-communicable diseases in hospital or other healthcare settings. *Biological Times, 4*(9), 20–21.

[7] Bartlett, A., Sanders, A. J., Ruge, F., Harding, K. G., & Jiang, W. G. (2016). Potential implications of interleukin-7 in chronic wound healing. *Experimental and Therapeutic Medicine*, *12*(1), 33–40. https://doi.org/10.3892/etm.2016.3263

[8] Boulton, A. J. M., Vileikyte, L., Ragnarson-Tennvall, G., & Apelqvist, J. (2005). The global burden of diabetic foot disease. *The Lancet*, *366*(9498), 1719–1724. https://doi.org/10.1016/S0140-6736(05)67698-2

[9] Bowers, K. J., Chow, E., Xu, H., Dror, R. O., Eastwood, M. P., Gregersen, B. A., Klepeis, J. L., Kolossvary, I., Moraes, M. A., Sacerdoti, F. D., Salmon, J. K., Shan, Y., & Shaw, D. E. (2006). Scalable algorithms for molecular dynamics simulations on commodity clusters. In *Proceedings of the 2006 ACM/IEEE Conference on Supercomputing (SC '06)* (Article 43). ACM. https://doi.org/10.1109/SC.2006.54

[10] Brem, H., & Tomic-Canic, M. (2007). Cellular and molecular basis of wound healing in diabetes. *Journal of Clinical Investigation*, *117*(5), 1219–1222. https://doi.org/10.1172/JCI32169

[11] Burgess, J. L., Wyant, W. A., Abdo Abujamra, B., Kirsner, R. S., & Jozic, I. (2021). Diabetic wound-healing science. *Medicina*, *57*(10), Article 1072. https://doi.org/10.3390/medicina57101072

[12] Calderón-Montaño, J. M., Burgos-Morón, E., Pérez-Guerrero, C., & López-Lázaro, M. (2011). A review on the dietary flavonoid kaempferol. *Mini-Reviews in Medicinal Chemistry*, *11*(4), 298–344. https://doi.org/10.2174/138955711795305335

[13] Chin, C.-H., Chen, S.-H., Wu, H.-H., Ho, C.-W., Ko, M.-T., & Lin, C.-Y. (2014). cytoHubba: Identifying hub objects and sub-networks from complex interactome. *BMC Systems Biology*, *8*(Suppl. 4), Article S11. https://doi.org/10.1186/1752-0509-8-S4-S11

[14] Daina, A., Michielin, O., & Zoete, V. (2017). SwissADME: A free web tool to evaluate pharmacokinetics, drug-likeness and medicinal chemistry friendliness of small molecules. *Scientific Reports*, *7*(1), 42717. https://doi.org/10.1038/srep42717

[15] Daina, A., Michielin, O., & Zoete, V. (2019). SwissTargetPrediction: Updated data and new features for efficient prediction of protein targets of small molecules. *Nucleic Acids Research*, *47*(W1), W357–W364. https://doi.org/10.1093/nar/gkz382

[16] Dallakyan, S., & Olson, A. J. (2015). Small-molecule library screening by docking with PyRx. *Methods in Molecular Biology*, *1263*, 243–250. https://doi.org/10.1007/978-1-4939-2269-7_19

[17] Deng, L., Du, C., Song, P., Chen, T., Rui, S., Armstrong, D. G., & Deng, W. (2021). The role of oxidative stress and antioxidants in diabetic wound healing. *Oxidative Medicine and Cellular Longevity*, *2021*, Article 8852759. https://doi.org/10.1155/2021/8852759

[18] Dinarello, C. A. (2018). Overview of the IL-1 family in innate inflammation and acquired immunity. *Immunological Reviews*, *281*(1), 8–27. https://doi.org/10.1111/imr.12621

[19] Eming, S. A., Krieg, T., & Davidson, J. M. (2007). Inflammation in wound repair: Molecular and cellular mechanisms. *Journal of Investigative Dermatology*, *127*(3), 514–525. https://doi.org/10.1038/sj.jid.5700701

[20] Falanga, V. (2005). Wound healing and its impairment in the diabetic foot. *The Lancet*, *366*(9498), 1736–1743. https://doi.org/10.1016/S0140-6736(05)67700-8

[21] Furman, B. L. (2021). Streptozotocin-induced diabetic models in mice and rats. *Current Protocols*, *1*(4), Article e78. https://doi.org/10.1002/cpz1.78

[22] Galiano, R. D., Michaels, J., V, Dobryansky, M., Levine, J. P., & Gurtner, G. C. (2004). Quantitative and reproducible murine model of excisional wound healing. *Wound Repair and Regeneration*, *12*(4), 485–492. https://doi.org/10.1111/j.1067-1927.2004.12404.x

[23] Ge, S. X., Jung, D., & Yao, R. (2020). ShinyGO: A graphical gene-set enrichment tool for animals and plants. *Bioinformatics*, *36*(8), 2628–2629. https://doi.org/10.1093/bioinformatics/btz931

[24] Guo, S., & DiPietro, L. A. (2010). Factors affecting wound healing. *Journal of Dental Research*, *89*(3), 219–229. https://doi.org/10.1177/0022034509359125

[25] Gurtner, G. C., Werner, S., Barrandon, Y., & Longaker, M. T. (2008). Wound repair and regeneration. *Nature*, *453*(7193), 314–321. https://doi.org/10.1038/nature07039

[26] Heberle, H., Meirelles, G. V., da Silva, F. R., Telles, G. P., & Minghim, R. (2015). InteractiVenn: A web-based tool for the analysis of sets through Venn diagrams. *BMC Bioinformatics*, *16*, Article 169. https://doi.org/10.1186/s12859-015-0611-3

[27] Heufler, C., Topar, G., Grasseger, A., Stanzl, U., Koch, F., Romani, N., Namen, A. E., & Schuler, G. (1993). Interleukin 7 is produced by murine and human keratinocytes. *Journal of Experimental Medicine*, *178*(3), 1109–1114. https://doi.org/10.1084/jem.178.3.1109

[28] Hopkins, A. L. (2008). Network pharmacology: The next paradigm in drug discovery. *Nature Chemical Biology*, *4*(11), 682–690. https://doi.org/10.1038/nchembio.118

[29] Jorgensen, W. L., Chandrasekhar, J., Madura, J. D., Impey, R. W., & Klein, M. L. (1983). Comparison of simple potential functions for simulating liquid water. *The Journal of Chemical Physics*, *79*(2), 926–935. https://doi.org/10.1063/1.445869

[30] Kilkenny, C., Browne, W. J., Cuthill, I. C., Emerson, M., & Altman, D. G. (2010). Improving bioscience research reporting: The ARRIVE guidelines for reporting animal research. *PLoS Biology*, *8*(6), e1000412. https://doi.org/10.1371/journal.pbio.1000412

[31] Leone, A., Spada, A., Battezzati, A., Schiraldi, A., Aristil, J., & Bertoli, S. (2015). Cultivation, genetic, ethnopharmacology, phytochemistry and pharmacology of *Moringa oleifera* leaves: An overview. *International Journal of Molecular Sciences*, *16*(6), 12791–12835. https://doi.org/10.3390/ijms160612791

[32] Li, S., & Zhang, B. (2013). Traditional Chinese medicine network pharmacology: Theory, methodology and application. *Chinese Journal of Natural Medicines*, *11*(2), 110–120. https://doi.org/10.1016/S1875-5364(13)60037-0

[33] Lipinski, C. A., Lombardo, F., Dominy, B. W., & Feeney, P. J. (2001). Experimental and computational approaches to estimate solubility and permeability in drug discovery and development settings. *Advanced Drug Delivery Reviews*, *46*(1–3), 3–26. https://doi.org/10.1016/S0169-409X(00)00129-0

[34] Livak, K. J., & Schmittgen, T. D. (2001). Analysis of relative gene expression data using real-time quantitative PCR and the $2^{-\Delta\Delta CT}$ method. *Methods*, *25*(4), 402–408. https://doi.org/10.1006/meth.2001.1262

[35] Loots, M. A. M., Lamme, E. N., Zeegelaar, J., Mekkes, J. R., Bos, J. D., & Middelkoop, E. (1998). Differences in cellular infiltrate and extracellular matrix of chronic diabetic and venous ulcers versus acute wounds. *Journal of Investigative Dermatology*, *111*(5), 850–857. https://doi.org/10.1046/j.1523-1747.1998.00381.x

[36] Lu, C., Wu, C., Ghoreishi, D., Chen, W., Wang, L., Damm, W., Ross, G. A., Dahlgren, M. K., Russell, E., Von Bargen, C. D., Abel, R., Friesner, R. A., & Harder, E. D. (2021). OPLS4: Improving force field accuracy on challenging regimes of chemical space. *Journal of Chemical Theory and Computation*, *17*(7), 4291–4300. https://doi.org/10.1021/acs.jctc.1c00302

[37] Mackall, C. L., Fry, T. J., & Gress, R. E. (2011). Harnessing the biology of IL-7 for therapeutic application. *Nature Reviews Immunology*, *11*(5), 330–342. https://doi.org/10.1038/nri2970

[38] Martin, P., & Nunan, R. (2015). Cellular and molecular mechanisms of repair in acute and chronic wound healing. *British Journal of Dermatology*, *173*(2), 370–378. https://doi.org/10.1111/bjd.13954

[39] Mazzucchelli, R., & Durum, S. K. (2007). Interleukin-7 receptor expression: Intelligent design. *Nature Reviews Immunology*, *7*(2), 144–154. https://doi.org/10.1038/nri2023

[40] Michaels, J., V, Churgin, S. S., Blechman, K. M., Greives, M. R., Aarabi, S., Galiano, R. D., & Gurtner, G. C. (2007). *db/db* mice exhibit severe wound-healing impairments compared with other murine diabetic strains in a silicone-splinted excisional wound model. *Wound Repair and Regeneration*, *15*(5), 665–670. https://doi.org/10.1111/j.1524-475X.2007.00273.x

[41] O'Boyle, N. M., Banck, M., James, C. A., Morley, C., Vandermeersch, T., & Hutchison, G. R. (2011). Open Babel: An open chemical toolbox. *Journal of Cheminformatics*, *3*(1), 33. https://doi.org/10.1186/1758-2946-3-33

[42] Okonkwo, U. A., & DiPietro, L. A. (2017). Diabetes and wound angiogenesis. *International Journal of Molecular Sciences*, *18*(7), Article 1419. https://doi.org/10.3390/ijms18071419

[43] Özay, Y., Güzel, S., Yumrutaş, Ö., Pehlivanoğlu, B., Erdoğdu, İ. H., Yildirim, Z., Türk, B. A., & Darcan, S. (2019). Wound healing effect of kaempferol in diabetic and nondiabetic rats. *Journal of Surgical Research*, *233*, 284–296. https://doi.org/10.1016/j.jss.2018.08.009

[44] Percie du Sert, N., Hurst, V., Ahluwalia, A., Alam, S., Avey, M. T., Baker, M., Browne, W. J., Clark, A., Cuthill, I. C., Dirnagl, U., Emerson, M., Garner, P., Holgate, S. T., Howells, D. W., Karp, N. A., Lazic, S. E., Lidster, K., MacCallum, C. J., Macleod, M., . . . Würbel, H. (2020). The ARRIVE guidelines 2.0: Updated guidelines for reporting animal research. *PLOS Biology*, *18*(7), e3000410. https://doi.org/10.1371/journal.pbio.3000410

[45] Rhea, L., & Dunnwald, M. (2020). Murine excisional wound healing model and histological morphometric wound analysis. *Journal of Visualized Experiments*, (162), Article e61616. https://doi.org/10.3791/61616

[46] Santana-Gálvez, J., Cisneros-Zevallos, L., & Jacobo-Velázquez, D. A. (2017). Chlorogenic acid: Recent advances on its dual role as a food additive and a nutraceutical against metabolic syndrome. *Molecules*, *22*(3), Article 358. https://doi.org/10.3390/molecules22030358

[47] Schneider, C. A., Rasband, W. S., & Eliceiri, K. W. (2012). NIH Image to ImageJ: 25 years of image analysis. *Nature Methods*, *9*(7), 671–675. https://doi.org/10.1038/nmeth.2089

[48] Shahzadi, S., Sani, K. Z., Shabbir, M. H., Afzal, M. A., Mukhtar, E., Ashraf, S., Mahmood, B., Zafar, M. N., Gull, S., Khan, S. S., & Rasheed, M. U. (2025). Chrononutrition and circadian rhythmicity: Exploring the temporal dynamics of nutrient intake in the regulation of glucose homeostasis and the therapeutic management of type 2 diabetes mellitus. *Review Journal of Neurological & Medical Sciences Review, 3*(8), 180–195. https://doi.org/10.5281/zenodo.17984112

[49] Shannon, P., Markiel, A., Ozier, O., Baliga, N. S., Wang, J. T., Ramage, D., Amin, N., Schwikowski, B., & Ideker, T. (2003). Cytoscape: A software environment for integrated models of biomolecular interaction networks. *Genome Research*, *13*(11), 2498–2504. https://doi.org/10.1101/gr.1239303

[50] Singh, A., Mishra, J. N., & Singh, S. K. (2019). Pharmacological importance of *Moringa concanensis* Nimmo leaf: An overview. *Asian Journal of Pharmaceutical and Clinical Research*, *12*(2), 27–31. https://doi.org/10.22159/ajpcr.2019.v12i2.28979

[51] Singh, A., Singh, S. K., Upadhyay, P. K., Mishra, J. N., & Vishwakarma, V. K. (2024). Characterization and extraction of bioactive compounds in ethanolic extract of *Moringa concanensis* Nimmo leaf using microwave-assisted and Soxhlet techniques. *Current Drug Therapy*, *19*(2), 233–238. https://doi.org/10.2174/1574885518666230522122556

[52] Singh, V. P., Bali, A., Singh, N., & Jaggi, A. S. (2014). Advanced glycation end products and diabetic complications. *The Korean Journal of Physiology & Pharmacology*, *18*(1), 1–14. https://doi.org/10.4196/kjpp.2014.18.1.1

[53] Stelzer, G., Rosen, N., Plaschkes, I., Zimmerman, S., Twik, M., Fishilevich, S., Stein, T. I., Nudel, R., Lieder, I., Mazor, Y., Kaplan, S., Dahary, D., Warshawsky, D., Guan-Golan, Y., Kohn, A., Rappaport, N., Safran, M., & Lancet, D. (2016). The GeneCards Suite: From gene data mining to disease genome sequence analyses. *Current Protocols in Bioinformatics*, *54*(1), 1.30.1–1.30.33. https://doi.org/10.1002/cpbi.5

[54] Sun, H., Saeedi, P., Karuranga, S., Pinkepank, M., Ogurtsova, K., Duncan, B. B., Stein, C., Basit, A., Chan, J. C. N., Mbanya, J. C., Pavkov, M. E., Ramachandaran, A., Wild, S. H., James, S., Herman, W. H., Zhang, P., Bommer, C., Kuo, S., Boyko, E. J., & Magliano, D. J. (2022). IDF Diabetes Atlas: Global, regional and country-level diabetes prevalence estimates for 2021 and projections for 2045. *Diabetes Research and Clinical Practice*, *183*, Article 109119. https://doi.org/10.1016/j.diabres.2021.109119

[55] Szklarczyk, D., Kirsch, R., Koutrouli, M., Nastou, K., Mehryary, F., Hachilif, R., Gable, A. L., Fang, T., Doncheva, N. T., Pyysalo, S., Bork, P., Jensen, L. J., & von Mering, C. (2023). The STRING database in 2023: Protein–protein association networks and functional enrichment analyses for any sequenced genome of interest. *Nucleic Acids Research*, *51*(D1), D638–D646. https://doi.org/10.1093/nar/gkac1000

[56] Trott, O., & Olson, A. J. (2010). AutoDock Vina: Improving the speed and accuracy of docking with a new scoring function, efficient optimization, and multithreading. *Journal of Computational Chemistry*, *31*(2), 455–461. https://doi.org/10.1002/jcc.21334

[57] Tukey, J. W. (1949). Comparing individual means in the analysis of variance. *Biometrics*, *5*(2), 99–114. https://doi.org/10.2307/3001913

[58] Vergara-Jimenez, M., Almatrafi, M. M., & Fernandez, M. L. (2017). Bioactive components in *Moringa oleifera* leaves protect against chronic disease. *Antioxidants*, *6*(4), Article 91. https://doi.org/10.3390/antiox6040091

[59] Zhao, W., Wang, B., & Li, S. (2024). Network pharmacology for traditional Chinese medicine in era of artificial intelligence. *Chinese Herbal Medicines*, *16*(4), 558–560. https://doi.org/10.1016/j.chmed.2024.08.004